REPORT DOCUMENTATION PAGE		Form Approved OMB NO. 0704-0188

The public reporting burden for this collection of information is estimated to average 1 hour per response, including the time for reviewing instructions, searching existing data sources, gathering and maintaining the data needed, and completing and reviewing the collection of information. Send comments regarding this burden estimate or any other aspect of this collection of information, including suggesstions for reducing this burden, to Washington Headquarters Services, Directorate for Information Operations and Reports, 1215 Jefferson Davis Highway, Suite 1204, Arlington VA, 22202-4302. Respondents should be aware that notwithstanding any other provision of law, no person shall be subject to any oenalty for failing to comply with a collection of information if it does not display a currently valid OMB control number.
PLEASE DO NOT RETURN YOUR FORM TO THE ABOVE ADDRESS.

1. REPORT DATE (DD-MM-YYYY) 05-05-2017	2. REPORT TYPE Final Report	3. DATES COVERED (From - To) 1-Sep-2013 - 30-Nov-2016

4. TITLE AND SUBTITLE	5a. CONTRACT NUMBER
Final Report: Nutrient-cycling Microbial Ecosystems: Assembly, Function and Targeted Design	W911NF-13-1-0284
	5b. GRANT NUMBER
	5c. PROGRAM ELEMENT NUMBER 611102
6. AUTHORS Rosalind Allen, Andrew Free	5d. PROJECT NUMBER
	5e. TASK NUMBER
	5f. WORK UNIT NUMBER

7. PERFORMING ORGANIZATION NAMES AND ADDRESSES	8. PERFORMING ORGANIZATION REPORT NUMBER
The University of Edinburgh Old College The University of Edinburgh -	

9. SPONSORING/MONITORING AGENCY NAME(S) AND ADDRESS (ES)	10. SPONSOR/MONITOR'S ACRONYM(S) ARO
U.S. Army Research Office P.O. Box 12211 Research Triangle Park, NC 27709-2211	11. SPONSOR/MONITOR'S REPORT NUMBER(S) 64052-MA.9

12. DISTRIBUTION AVAILIBILITY STATEMENT
Approved for Public Release; Distribution Unlimited

13. SUPPLEMENTARY NOTES
The views, opinions and/or findings contained in this report are those of the author(s) and should not contrued as an official Department of the Army position, policy or decision, unless so designated by other documentation.

14. ABSTRACT
The bioremediation of contaminated sites relies on microbial communities. Different populations of microbes undertake different chemical transformations, converting potentially harmful chemicals via a series of intermediates, to harmless waste products. This shuttling of chemical elements between their oxidized and reduced forms is known as nutrient cycling. We have used a combination of mathematical models and microcosm experiments to understand how nutrient-cycling microbial populations establish themselves, respond to environmental changes and how they can be optimised for use in bioremediation

15. SUBJECT TERMS
nutrient-cycling, microbial ecology, mathematical modelling

16. SECURITY CLASSIFICATION OF:			17. LIMITATION OF ABSTRACT	15. NUMBER OF PAGES	19a. NAME OF RESPONSIBLE PERSON Rosalind Allen
a. REPORT UU	b. ABSTRACT UU	c. THIS PAGE UU	UU		19b. TELEPHONE NUMBER +44-131-6517

Agency Code:

Proposal Number: **Agreement Number:**

Organization:
Address: , ,
Country:
DUNS Number: EIN:
Report Date: Date Received:
 for Period Beginning and Ending
Title:
Begin Performance Period: **End Performance Period:**
Report Term: -
Submitted By: Email:
                                                    Phone:

Distribution Statement: -

STEM Degrees: **STEM Participants:**

Major Goals:

Accomplishments:

Training Opportunities:

Results Dissemination:

Plans Next Period:

Honors and Awards:

Protocol Activity Status:

Technology Transfer:

Final Progress Report   April 2017

Foreword
This document details the scientific progress made during the 3-year grant.

Results published or under review
1. Mathematical modelling shows that biogeochemical feedbacks in microbial communities can cause oxic-anoxic regime shifts (Bush et al, in collaboration with Profs Huisman and Muyzer, University of Amsterdam, manuscript under review at Nature Communications)
2. Mathematical modelling shows that nonlinearities in microbial population dynamics can cause redox regime shifts (Bush et al, Biogeosciences 12, 3717-3724 (2015))
3. Microcosm experiments show that initially identical replicate communities can diverge into apparent alternative stable states (Pagaling et al, manuscript under review at Environmental Microbiology)
4. Microcosm experiments show that selection history affects the predictability of community development (Pagaling et al, ISME J. 8, 19-30 (2014)).

Results still to be published

1. Experiments show the time-dependent development of microbial nutrient-cycling ecosystems, for different nutrient conditions, in terms of both community structure and chemical composition.
2. Experiments show response of steady-state microbial microcosm communities to environmental change, in terms of community structure and chemical composition.
3. Experiments show response of microcosm communities to addition of the pollutant PCP and also to addition of the PCP biodegrading organism *D. hafniense* PCP-1.
4. Development of a mathematical model to mimic the effects of adding organisms that can mediate reductive biodegradation to a nutrient-cycling microbial community.

List of appendices, illustrations and tables
- Figure 1. Replicate microcosms created from freshwater pond sediment and water, supplemented by cellulose and sulfate.
- Figure 2. Analytical predictions of a '2 population' model for a biogeochemical cycle showing that it predicts redox regime shifts as a function of the reductive and oxidative driving forces.
- Figure 3. Results for a 4-population, 2-box mathematical model of a biogeochemical cycle, showing that this model also predicts redox regime shifts.
- Figure 4: Schematic diagram showing the microbial populations, chemical species and their interactions, in our mathematical model of a nutrient-cycling ecosystem in which feedbacks lead to alternate stable states.
- Figure 5: Dynamical trajectories generated by the model for Figure 4, showing that different initial system states can produce very different final communities, for the same set of parameters.
- Figure 6: Hysteresis in a nutrient-cycling microbial community. (a): Prediction of our mathematical model of Figure 4; as oxygen diffusivity is gradually increased the system remains for a long time in an anoxic state; as oxygen diffusivity is gradually decreased starting from the oxic state, the system remains for a long time in the oxic state. (b): Data

gathered from Lake Vechten in the Netherlands, showing a similar hysteretic phenomenon.

- Figure 7. Experimental results for microcosm structure as a function of time. Summary plot (a), NMDS plot (b), and measure of community diversity (c), showing community composition in our microcosm communities as a function of time, as determined by 16S rRNA gene sequencing.
- Figure 8: Experimental results for steady-state microcosms with varying environmental parameters. Diversity (as measured by Shannon Index) is plotted versus relative abundance in our set of microcosms with different environmental conditions, for the three functional groups: phototrophic sulfur bacteria, sulfate reducing bacteria and oxygenic phototrophic bacteria. We see different trends for the different groups, suggesting that their community structure may be driven by different ecological mechanisms.
- Figure 9: Schematic illustration of our mathematical model describing a nutrient cycling microbial ecosystem supplemented by reductive dehalogenators.
- Figure 10: Experimental results for microcosms supplemented with PCP and *D. hafniense*: the persistence of *D. hafniense* in the microcosms depends on the level of added sulfate.

- Appendix 1: Equations corresponding to our 4-population, 2-box mathematical model.
- Appendix 2: Equations used to describe our mathematical model for the nutrient-cycling microbial ecosystem with alternate stable states.

Statement of the problem studied

The bioremediation of contaminated sites relies on microbial communities. Different populations of microbes undertake different chemical transformations, converting potentially harmful chemicals via a series of intermediates, to harmless waste products [1-4]. This shuttling of chemical elements between their oxidized and reduced forms is known as nutrient cycling [5]. Nutrient cycling is not only important in bioremediation, but is also an essential feature of the Earth's biogeochemical cycles, and thus forms a key component of global Earth-system models [6-8]. Improving our approaches to bioremediation, and our basic understanding of how biogeochemical cycles work, requires us to be able to predict the response of nutrient-cycling microbial communities to environmental changes such as addition of pollutants. Yet despite a wealth of new information emerging from DNA sequencing technologies [9], our basic understanding of the principles underlying the structure and function of these microbial communities remains very poor [10,11]. The overarching goal of our project was to reveal fundamental principles underlying the assembly and function of nutrient-cycling microbial communities, using a combination of mathematical modeling and laboratory experiments. Our specific aims were:

1. To characterize experimentally the dynamical changes that occur during the development of a microbial nutrient-cycling ecosystem and to develop a mathematical model that can reproduce these changes.
2. Using this insight, to predict how these systems respond to environmental change and to test these predictions experimentally.
3. To apply these principles to the targeted design of microbial communities for applications in bioremediation.

To achieve these aims, our project combined theoretical and experimental work. On the theoretical side, our models are based on ordinary differential equations, in which variables represent the population densities of different microbial metabolic types, and the concentrations of key chemical species [12,13]. The growth of a given population depends on the concentration of its food sources, and as it grows it excretes waste products that can be used as food by other populations [14,15]. On the experimental side, we have used laboratory microcosms, made from pond sediment and water, supplemented by carbon and sulfur sources [16]. Over several months these microcosms develop into vertically stratified, stable, nutrient-cycling communities. We are able to track the development of chemical gradients within the microcosms using voltammetry [17], and to track the microbial community composition by extraction, fingerprinting and sequencing of DNA [18].

Summary of the most important results

<u>Aim 1: Dynamical development of a nutrient-cycling ecosystem</u>

Aim 1.1: Experimental characterization of microbial ecosystem development

We have established a complete set of chemical data (sulfide and oxygen profiles) and microbial community composition data (16S metataxonomic data via Illumina sequencing) on 11 microcosms which were set up in late 2013, and monitored weekly for 30 weeks (Figure 1 and Figure 7). The microcosms were set up with three different levels of added cellulose, which we know has a drastic effect on microcosm development. We incubated these microcosms under fixed light and temperature conditions and monitored their development in terms of chemical composition (sulfide and oxygen profiles) on a weekly basis for a period of 30 weeks. We also obtained samples for DNA analysis of the microbial community composition, non-destructively using a thin corer. As the microbial community develops, sulfur-reducing bacteria convert the sulfate to sulfide, driven by acetate and hydrogen which are released by the decomposition of the cellulose. Thus tracking the production of sulfide provides a measure of the functional changes occurring in this ecosystem. Our first observation was that the total amount of sulfide in our microcosms peaks at a time and level which depends on the amount of carbon source added. We also obtained much more detailed information on the species composition of our microcosms, by both DGGE fingerprinting and Illumina sequencing of samples taken non-destructively from our microcosms. The results show that species composition changes strongly in time, and with the initial cellulose and sulfate concentrations (Figure 7). They also reveal large blooms of *Chlorobi* (green sulfur bacteria) in the microcosms with higher initial cellulose concentrations, confirming the importance of the sulfur cycle in these ecosystem. Plotting the sequence data as a non-metric multidimensional scaling (NMDS) plot, in which the distance between two points approximately represents the difference in species composition between two samples (Figure 7), we see that microcosms with different initial cellulose concentrations follow very distinct dynamical trajectories. All communities change initially rapidly, and then more slowly, over the 15 week time period. The greater the amount of initial added cellulose, the more the community composition changes compared to its initial inoculating sediment. Combining these observations with our chemical data, which shows very different dynamical changes in sulfide concentration depending on the amount of initial cellulose, suggests that the production of sulfide by sulfur reducing microbes, driven by reducing equivalents generated by cellulose degradation, may

ultimately drive community development. Intriguingly, our data also reveals that species diversity correlates inversely with sulfide concentration, initially decreasing as our microcosms develop, but later increasing again. This effect is most pronounced for the experiments with the largest amount of added cellulose; suggesting that the initial diversity loss may be driven by the production of sulfide.

We have also performed an experiment (revised manuscript submitted to *Environmental Microbiology*) in which 100 replicate microcosms were set up, and sampled after either 8 weeks' or 16 weeks' development. These microcosms show divergence in community composition as a function of time (which we do not see in larger microcosms), and appear to form alternative stable states, diverging in time in a system size-dependent manner. The alternative stable states are characterized by differences in the degrader communities; one group of steady state microcosm communities is enriched with specific *Firmicutes* species, while the other is enriched with specific *Bacteroidetes*. The communities dominated by members of these two phyla also contain distinct populations of sulphate-reducing bacteria. This biomodality in community composition appears to arise during recovery from a low-diversity state that follows initial cellulose degradation and sulphate reduction. These results are significant because relatively few observations of alternative stable states have been reported for microbial ecosystems, even though they are rather widely reported for macro-ecosystems.

Aim 1.2: Mathematical modeling of ecosystem development

During the course of this project we have developed two complementary frameworks for modelling ecosystem development in nutrient-cycling microbial communities. Both models are based on ordinary differential equations for the dynamics of the various microbial populations and chemical species in our ecosystems. The first model focuses on the non-linearity of microbial growth kinetics; the second focuses on feedbacks between the growth of different microbial functional types.

Model 1: non-linear growth (Appendix 1). We have completed an extensive theoretical study of perhaps the simplest possible mathematical model for a nutrient-cycling ecosystem: a model in which two populations exchange metabolites, population 1 converting the reduced form of a chemical species (which we denote s_r) into its oxidized form (s_o) and population 2 performing the reverse transformation. This model, though simple, actually provides a rather generic representation of many of the Earth's biogeochemical cycles. For this model, the differential equations describing the growth of the two populations and the concentrations of s_o and s_r can be solved analytically for the steady state (Appendix 1). Importantly, we find that the model undergoes a transition between a "reduced" ecosystem state (with high levels of s_r) and an "oxidized" ecosystem state (with high levels of s_o) as we vary the maximal growth rate of either the reducing or the oxidizing microbial population (Figure 2). We termed this transition a "redox regime shift" in analogy with sharp transitions in ecosystem state, known as regime shifts, which have been observed in other ecosystems (eg the shift between temperate and desert states for savanna ecosystems). We believe that this transition is relevant to our experiments, because varying the maximal growth rate of the reducer population provides a proxy for changes in the levels of acetate/hydrogen, which are in turn produced by the degradation of cellulose. Thus, varying the concentration of cellulose in our experiments corresponds to varying the maximal

growth rate parameter in our very simple 2-population model. The advantage of using such a simple model is that we can obtain analytical solutions, which allow us to access the fundamental mechanisms underlying the regime shifting behavior. We find that the regime shift occurs when the microbial population size becomes saturated, so that a population can no longer respond to a change in the level of its redox substrate; thus these regime shifts are a fundamental consequence of the non-linearity of the microbial population dynamics.

To verify that this regime shifting behavior is actually relevant for real ecosystems, we also simulated a more detailed, 2-box model, including 4 microbial populations (Figure 3). In this model, cellulose degraders, which release acetate from cellulose, and photosynthesizers, which produce oxygen when stimulated by light, are explicitly included. This model mimics spatial heterogeneity in a basic way by defining separate spatial regions representing the upper, oxic zone and the lower, anoxic zone in our microcosms. These regions are coupled by chemical diffusion and within each region we assume that the system is well-mixed. We have shown that this model also predicts a drastic change in ecosystem state in response to gradual changes in environmental parameters (here the level of light intensity and concentration of organic matter). We also showed that the parameters for which such redox regime shifts are predicted by the model are realistic for nutrient cycling populations in the natural environment.

This work, which has been published in *Biogeosciences*, shows that proper consideration of non-linearities in the equations modelling microbial population dynamics can have drastic effects on the model predictions. This is an important conclusion given that microbial populations in large-scale biogeochemical models are usually modelled very crudely.

Model 2: feedbacks between functional groups (Appendix 2) We have also collaborated with Prof. Jef Huisman and Prof. Gerard Muyzer (University of Amsterdam, The Netherlands), to develop a second mathematical model, that explains how alternative stable states can arise in a nutrient-cycling microbial ecosystem. The model describes the coupled population dynamics of cyanobacteria, sulfate-reducing bacteria and phototrophic sulfur bacteria, as found in our microcosms. In the model, cyanobacteria produce oxygen, which inhibits the sulfate-reducing bacteria and the phototrophic sulfur bacteria. Conversely, the sulfate-reducing bacteria produce sulfide, which inhibits the cyanobacteria. The phototrophic bacteria oxidize sulfide, creating a sulfur cycle. Sulfur can also be oxidized abiotically, providing an alternative cycling mechanism (Figure 4). Numerical solution of this model shows clearly that, in some regimes of parameter space, the model has two alternate stable states, one of which is oxic and rich in cyanobacteria, and the other of which is anoxic and rich in sulfate-reducing bacteria. The anoxic state can take two forms, depending on the parameters; a form in which phototrophic bacteria coexist with sulfate-reducing bacteria, and a form in which sulfide is oxidized abiotically, so that only sulfate-reducing bacteria are abundant. Figure 5 shows that the model dynamics leads to these very different final states when we make a small change in the initial population abundances.

Aim 2: Sensitivity to environmental change

Aim 2.1: Predict how our ecosystems respond to changes in carbon, sulfur and light

Our feedback-based mathematical model sheds new light on how nutrient-cycling microbial ecosystems may respond to environmental changes. Specifically, the model predicts the existence of hysteresis: changes in ecosystem state in response to parameter changes, that are not reversible when the parameter change is reversed. This is illustrated in Figure 6a, where we show the results of a series of simulations of the model, where in each successive simulation we increase the oxygen diffusivity, initiating the new simulation from the steady state of the previous simulation. This mimics an experiment in which oxygen diffusivity is slowly increased (eg by changing the temperature). Initially, for low oxygen diffusivity, the system is anoxic (oxygen concentration is low). As oxygen diffusivity is increased, the oxygen concentration increases slightly (blue line in Figure 6a), before making a sudden transition to a much more oxic state (red line in Figure 6a). Starting from the final, oxic, state of this series of simulations, we then gradually decrease the oxygen diffusivity, in the same manner. The red line shows the results: oxygen concentration remains high over a range of oxygen diffusivities where we obtained the anoxic state in our previous set of simulations. Eventually we do see a transition back to the anoxic state.

This prediction of hysteresis has important consequences for the management of freshwater lakes. For example, if hysteresis is present then attempts to reoxygenate anoxic lakes will require much more oxygen to be pumped into the deep water than a simple calculation might suggest. Interestingly, we have evidence that hysteresis does occur in a freshwater lake that is being studied by our Dutch collaborators: Lake Vechten in the Netherlands. This lake is typically mixed and oxic during the winter (when oxygen diffusivity is high) and stratified (with an upper oxic layer) during the summer, when oxygen diffusivity is low. Figure 6b shows a plot of oxygen concentration at a depth of 7m as a function of the stratification of the lake; the data points were sampled at different times over the course of a year. When measurements started in March (blue data point), the lake was mixed and oxic. A transition to a stratified state occurred over the next few months, and the oxygen concentration at 7m dropped dramatically. However, over the winter months, when the lake mixed again, it remained anoxic for several weeks, before making a sudden transition back to the mixed oxic state. Thus the lake shows clear evidence of hysteresis. Metataxonomic analysis of samples from the lake community over time shows negative correlations in the abundance of cyanobacterial with sulfate-reducing bacteria and phototrophic sulfur bacteria, while the two latter groups are positively correlated; also in agreement with the mathematical model. This work is under review for publication in *Nature Communications*.

Aim 2.2: Compare the model predictions to experimental data

As explained in the previous section, we have been able, at least qualitatively, to compare the prediction of hysteresis from our mathematical model to field data from a freshwater lake. We have also been carrying out microcosm experiments to investigate the effects of environmental change on nutrient-cycling microbial communities, as detailed in our previous reports.

We have also performed microcosm experiments in which we have obtained and analyzed a complete set of data for a series of microcosms containing different concentrations of cellulose and sulfate. After incubating these microcosms for 16 weeks, we measured vertical profiles of sulfide and oxygen, and took samples for DNA analysis (via Illumina 16S rRNA gene sequencing). We also analyzed the DNA sequence data in terms of microbial functional groups,

finding that different functional groups showed different responses to environmental change: for example sulfate reducers maintain stable abundance and diversity in response to changes in sulfate and cellulose, but oxygenic phototrophs show a collapse in diversity as cellulose concentration increases. We believe that these results may be useful in understanding the niche structure of microbial communities. Within a particular microbial functional group, we suppose that individual taxa occupy specific niches (for example defined by a particular pH range, spatial location etc). In our experiment, we can track how the occupation of these niches changes as we change the environmental conditions. For example for sulfate-reducing bacteria, we see that diversity is higher in microcosms where the sulfate-reducing population is higher (diversity is positively correlated with abundance); Figure 8a. This suggests that more niches are present in microcosms with higher sulfate reducer diversity. However, we observe the opposite for phototrophic sulfur bacteria: diversity is actually lower in microcosms where phototrophic sulfur bacteria are more abundant; Figure 8b. This can be explained by a picture in which a few niches expand in size as the total population expands, but most niches remain the same. For oxygenic phototrophs, we see yet another scenario: diversity remains the same as the abundance increases; Figure 8c. This is consistent with a picture in which the number of niches remains the same but they all increase in size proportionally. To our knowledge, this is the first observation to suggest that the ecology of different microbial functional groups might be fundamentally different – suggesting that attempts to apply "ecological theory" as defined for macro-organisms, to microbial communities, may well be over-simplistic. We are working on a manuscript describing these results.

Aim 3: Targeted optimization of microbial communities for bioremediation

We have established a model system for studying the biodegradation of the pollutant PCP in our microcosms, using the biodegrading organism *D. hafniense*, and assays for both *D. hafniense* (by PCR) and PCP (using gas chromatography-mass spectrometry (GC-MS)). This system is interesting because *D. hafniense* requires hydrogen as an electron donor. The sulfate reducers, which play a key role in our microcosms, may inhibit *D. hafniense*, by competing for hydrogen (which they use to reduce sulfate). However, some literature suggests that sulfate reducers may under some circumstances actually aid the growth of *D. hafniense* by producing hydrogen (which happens when they grow fermentatively). Motivated by this potentially interesting conflict, we have set up a range of microcosms with different amounts of added sulfate, some of which have been supplemented by PCP and / or *D. hafniense*. From a practical point of view, an especially interesting question concerns the length of time that a population of *D. hafniense* is maintained in the community. Previous studies of bioaugmentation (in which a pollutant-degrading organism is added to a microbial community) suggest that the added population tends to die out within a few days, limiting the usefulness of the method for pollutant degradation. Our data, in contrast, suggest that *D. hafniense* can persist in our microcosms for many weeks.

Aim 3.1: Theoretical predictions of optimal conditions for PCP degradation
We have extended our "feedback" mathematical model (Figure 4), to include a population of reductive dehalogenators (representing *D. hafniense*). This population consumes PCP, competes with sulfate-reducing bacteria for hydrogen, and competes with all other organisms for phosphorous. It is also inhibited by oxygen (since *D. hafniense* is anaerobic). The extended model structure is shown in Figure 9. Our model predicts a strong dependence of the ecosystem

state on the total amount of sulfur that is present. At low total sulfur, cyanobacteria dominate and the system is oxic, with no PCP degradation. At higher levels of sulfur, the action of sulfate-reducing bacteria causes the system to become anoxic. If the sulfur level is not too high then sulfate reducers are eventually outcompeted by reductive dehalogenators, due to the competition for hydrogen. However if the level of sulfur is very high then the sulfate reducers will outcompete the reductive dehalogenators, leading to a final state with a sulfur cycle but without PCP degradation. Thus, the model predicts that PCP degradation, and persistence of *D. hafniense*, will only occur at intermediate concentrations of added sulfur.

Aim 3.2: Experimental measurements of PCP degradation

We have carried out experiments using microcosms supplemented with PCP and *D. hafniense*, compared to unsupplemented microcosms, in the presence of different levels of added sulfate. Our results show the supplementation with PCP affects community structure drastically, and, excitingly, that *D. hafniense* can persist in our microcosms over long times (Figure 10). This is in contrast to many attempts at bioaugmentation, including with *D. hafniense* in soil microcosms, in which the added organism is rapidly lost. Consistent with our model, we see that *D. hafniense* is lost more rapidly from microcosms without added sulfate than from microcosms to which a low concentration of sulfate has been added. We also see strong changes in microbial community composition depending on the levels of added PCP and sulfate. We have also just obtained sequence data from a final experiment, completed last year, in which a higher level of sulfate was added to PCP- and *D. hafniense*-supplemented microcosms. With the assistance of a Masters student, we will be analyzing these data over the next few months to determine whether, as predicted, the high level of sulfate allows the sulfate reducers to out-compete *D. hafniense* and shorten its persistence in the microcosm system.

Taken together, our modelling and simulation results on the PCP-*D. hafniense* microcosm system provide new insights into the mechanisms that may come into play when reductive dehalogenators are added to a nutrient-cycling microbial ecosystem. It is clear from our results that understanding the structure and function of nutrient-cycling microbial communities can indeed lead to targeted strategies for bioremediation: producing much longer persistence of added pollutant-degrading organisms than has been achieved before.

Bibliography
[1] Rittmann, B. E., et al. (2006), 'A vista for microbial ecology and environmental biotechnology', *Environ Sci Technol,* 40 (4), 1096-103.
[2] Adriaens, P., Gruden, C. and McCormick, M. L. (2007), 'Biogeochemistry of halogenated hydrocarbons' *Treatise on Geochemistry* 9, 1-35.
[3] Beaudet, R., et al. (1998), 'Anaerobic biodegradation of pentachlorophenol in a contaminated soil inoculated with a methanogenic consortium or with *Desulfitobacterium frappieri* strain PCP-1', *Appl Microbiol Biotechnol,* 50 (1), 135-41.
[4] De Wildeman, S., et al. (2004), 'Complete lab-scale detoxification of groundwater containing 1,2-dichloroethane', *Appl Microbiol Biotechnol,* 63 (5), 609-12.
[5] Madigan, R.T., et al. (2011), '*Brock Biology of Microorganisms*' (Thirteenth edn.; London: Pearson Prentice Hall).

[6] Brimblecombe, P. (2007), 'The global sulfur cycle' *Treatise on Geochemistry* 8, 645-682.

[7] Houghton, R. A. (2007), 'The contemporary carbon cycle' *Treatise on Geochemistry* 8, 473-513.

[8] Falkowski, P. G. (2007), 'Biogeochemistry of primary production in the sea' *Treatise on Geochemistry* 8, 185-213.

[9] Pedros-Alio, C. (2012), 'The Rare Bacterial Biosphere', *Ann Rev Marine Sci,* 4, 449-66.

[10] Prosser, J. I., et al. (2007), 'The role of ecological theory in microbial ecology', *Nat Rev Microbiol,* 5 (5), 384-92.

[11] Prosser, J. I. (2012), 'Ecosystem processes and interactions in a morass of diversity', *FEMS Microbiol Ecol*, 81 (3), 507-19.

[12] Murray, J. D. (2002), '*Mathematical Biology I. An Introduction*' (3rd Edition), Springer-Verlag.

[13] Bazin, M. J., and Prosser, J. I. (1988) '*Physiological Models in Microbiology, volumes 1 and 2*', CRC Press.

[14] Khatri, B.S., Free, A., and Allen, R.J. (2012), 'Oscillating microbial dynamics driven by small populations, limited nutrient supply and high death rates', *J Theor Biol,* 314, 120-9.

[15] Jin, Q. S., and Bethke, C. M. (2005) 'Predicting the rate of microbial respiration in geochemical environments', *Geochim Cosmochim Acta* 69 (5), 1133-1143.

[16] Pagaling, E., Strathdee, F., Spears, B.M., Cates, M. E., Allen, R. J., and Free, A. (2014), 'Community history affects the predictability of microbial ecosystem development', *ISME J.* 8, 19-30.

[17] Taillefert, M., Luther, G. W., and Nuzzio, D. B. (2000) 'The application of electrochemical tools for in situ measurements in aquatic systems', *Electroanalysis* 12 (6), 401-12.

[18] Caporaso, J. G., et al. (2010), 'QIIME allows analysis of high-throughput community sequencing data', *Nature Meth,* 7 (5), 335-36.

Figure 1

Photograph of the microcosms which we have been tracking dynamically as they undergo community assembly. This photograph was taken 10 weeks into the experiment. The different colored labels indicate microcosms with different added amounts of cellulose.

Fully biotic cycle

Biotic-abiotic cycle
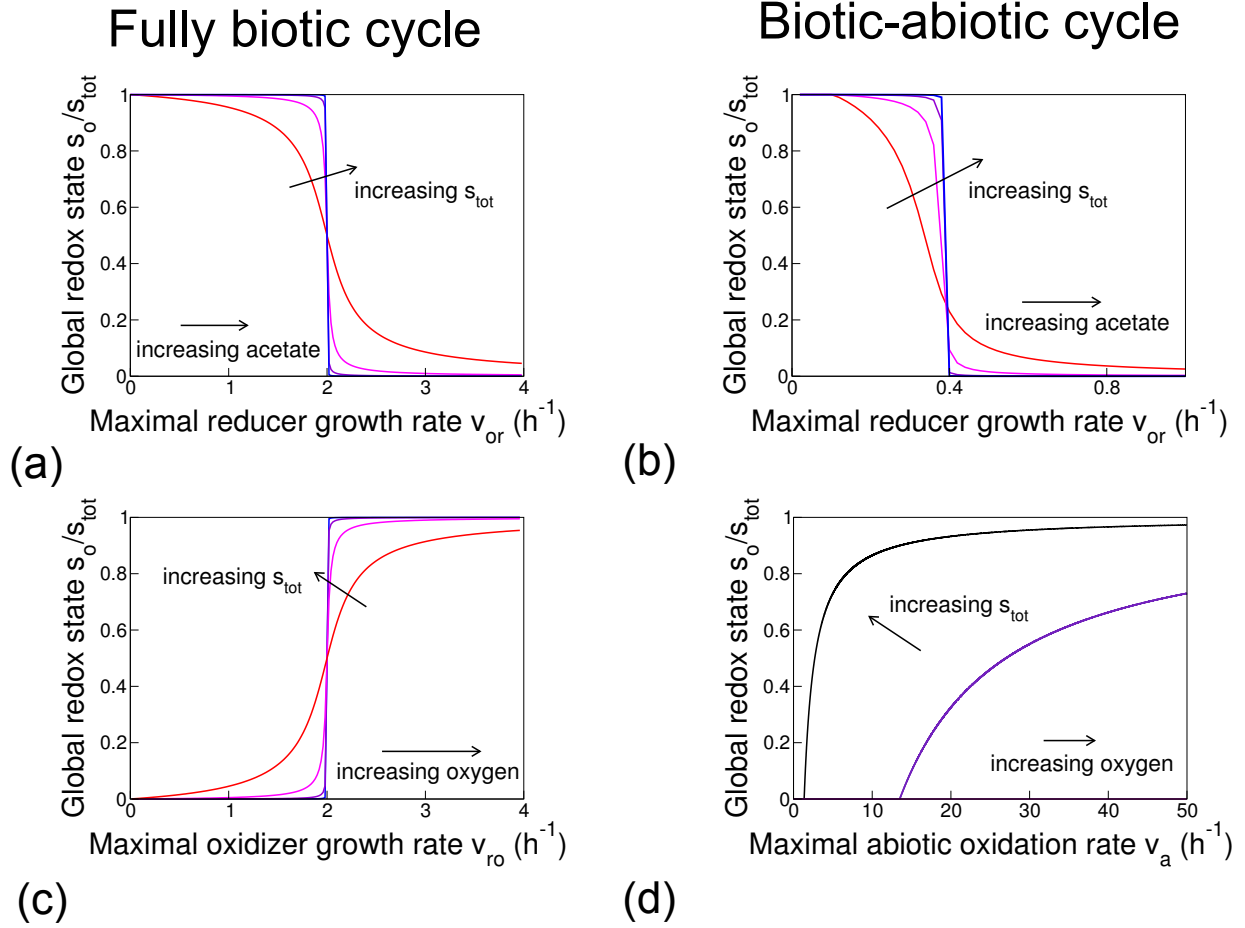
Figure 2

Redox regime shifts in model nutrient cycles, obtained by analytical solution of a simple model. In this model, in the "fully biotic case", one population transforms a chemical from its oxic form s_o to its anoxic form s_r and another performs the reverse transformation. In the "biotic-abiotic case", a microbial population performs the oxic to anoxic transformation but the anoxic to oxic transformation is mediated by an abiotic reaction. The global redox state, as measured by the oxidized fraction s_o/s_{tot}, predicted by the steady-state solution of the model equations for the fully biotic cycle (a and c) or the biotic-abiotic cycle (b and d) is plotted as a function of parameters that form proxies for the degree of reductive or oxidative driving. These parameters are: for reductive driving, the maximal growth rate of the reductive population, v_{or} (a and b), and, for oxidative driving, either the maximal growth rate of the oxidative population v_{ro} (c) or the maximal abiotic oxidation rate v_a (d). The results show a shift between oxidized and reduced ecosystem states as a threshold in reductive or oxidative driving is crossed; the sharpness of this transition increases with the concentration of the chemical species being cycled, s_{tot} (in panels a to c, red to blue lines; red: $s_{tot} = 20\mu M$, pink: $s_{tot} = 0.2mM$, purple: $s_{tot} = 2mM$ blue: $s_{tot} = 20mM$; in panel d, black line $s_{tot} = 2M$: dark purple line: $s_{tot} = 200mM$).
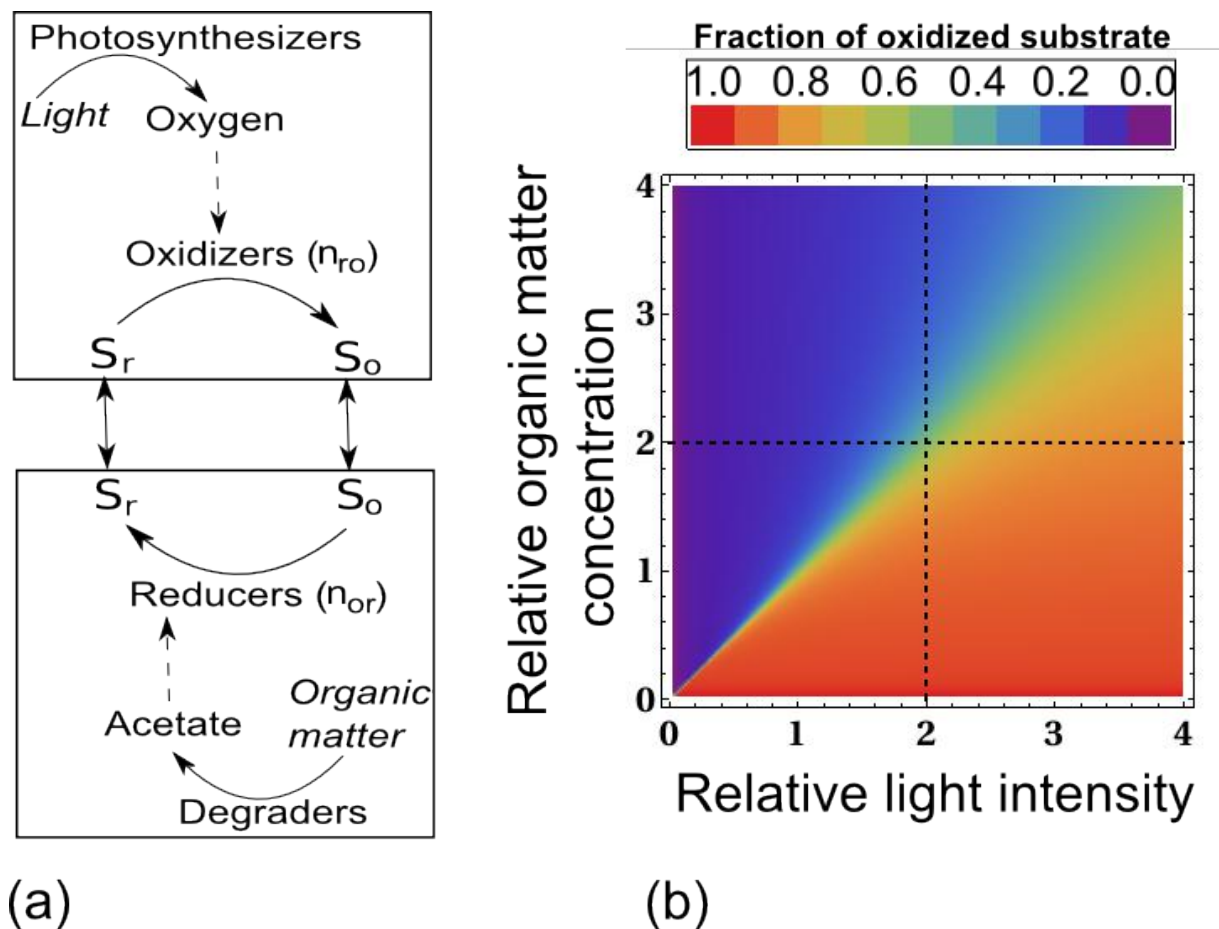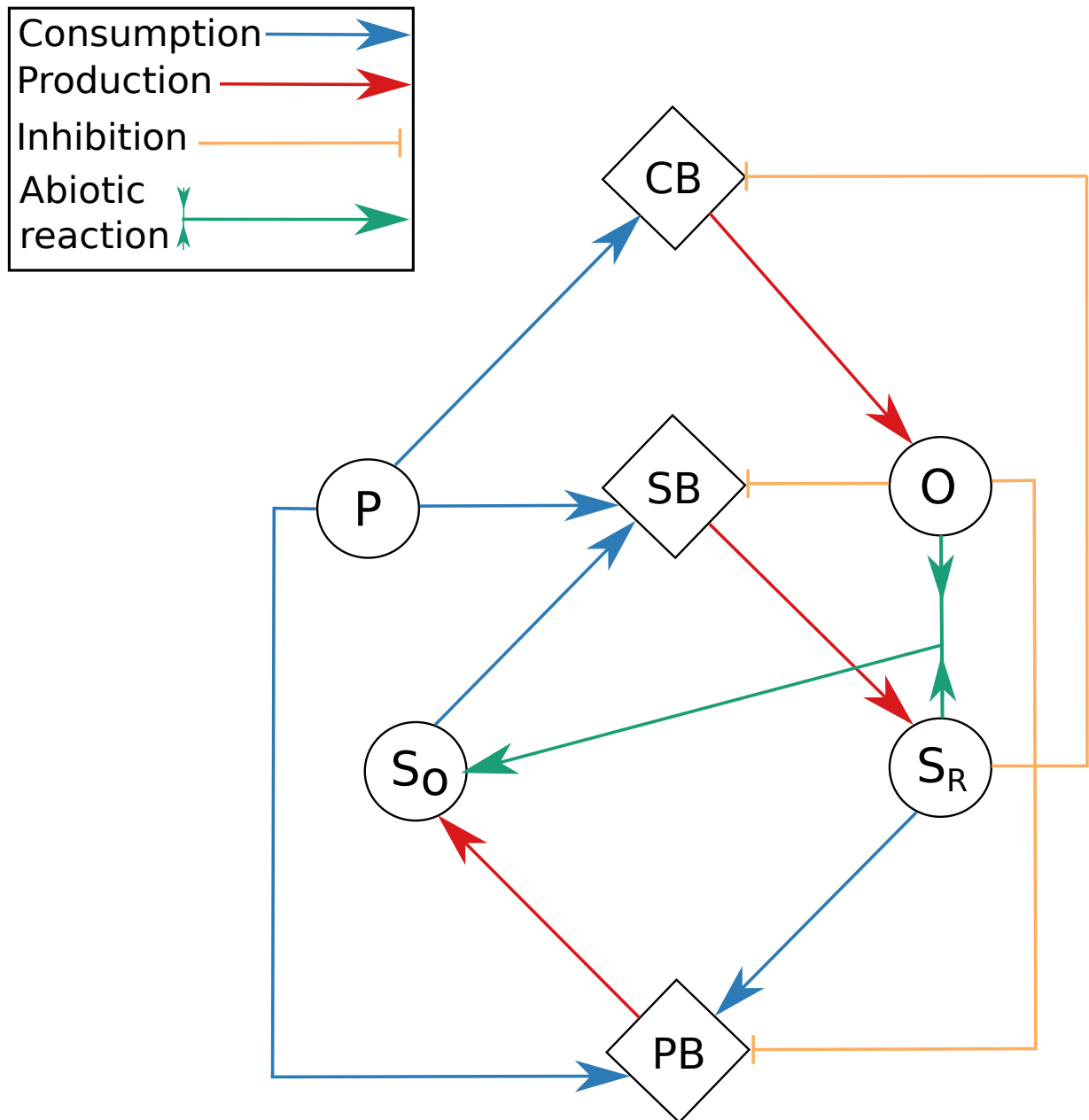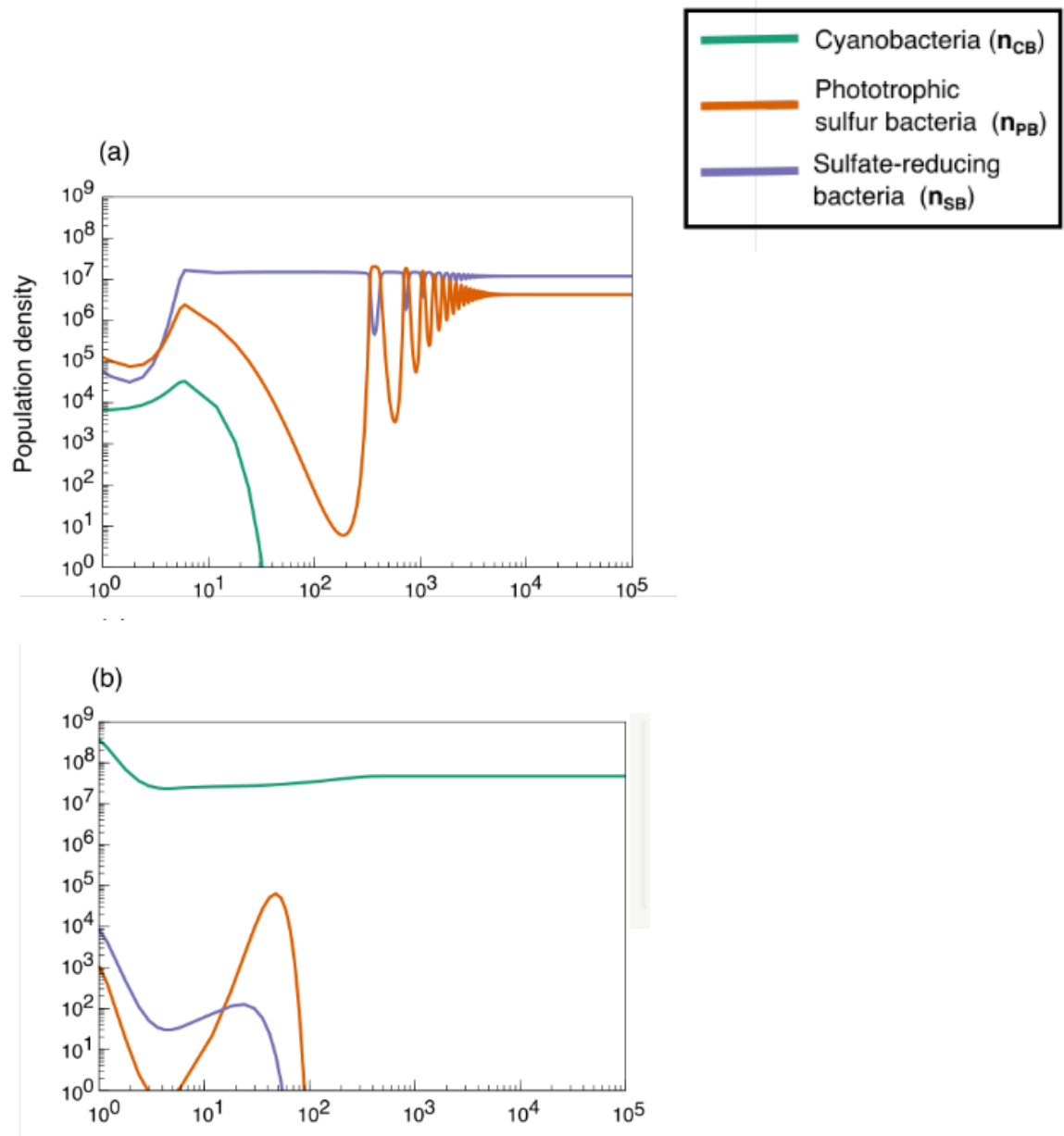
Figure 3

The "four-population, two-box" mathematical model and its predictions for redox regime shifts. (a) Illustration of the model. Oxidative and reductive processes take place in separate spatial zones, linked by chemical diffusion. The model explicitly represents the population dynamics of microbial photosynthesizers, decomposers, reducers and oxidizers, and the chemical dynamics of oxygen, s_o, s_r and acetate. Light intensity and organic matter availability are treated as control parameters. The dynamical equations corresponding to the model are integrated numerically to find the steady-state solution. (b) Steady-state solution of the complete ecosystem model, obtained numberically, plotted as a function of the control parameters, light intensity (relative to the typical value 10 μEinstein s^{-1}m^{-2}) and organic matter concentration (relative to the typical value 100 mg cm^{-3}). The color represents the global redox state (see color key). The model shows redox regime shifts as the organic matter concentration is varied at fixed light intensity (vertical dashed line) or as the light intensity is varied at fixed organic matter concentration (horizontal dashed line).
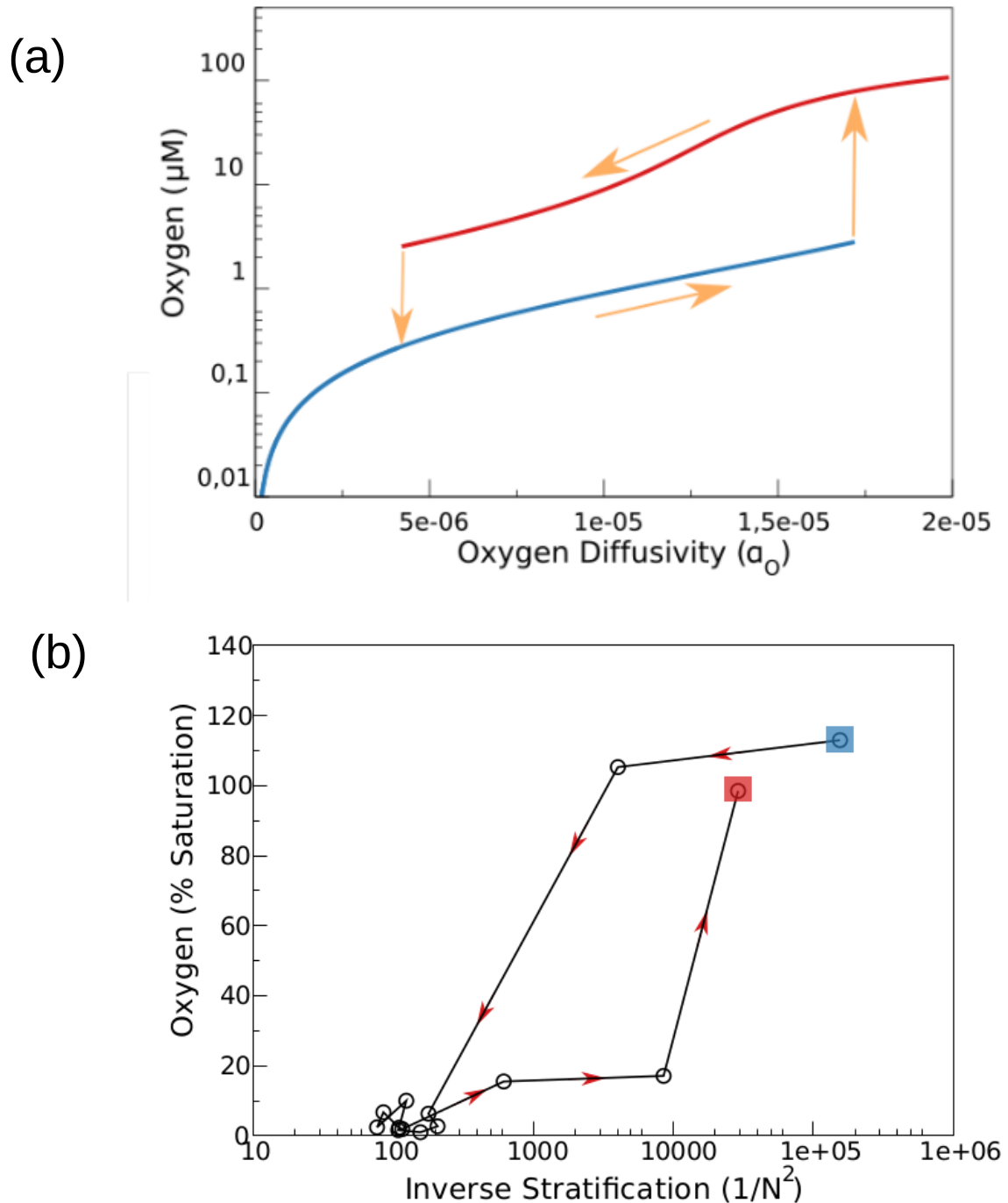
Figure 4

A schematic diagram of our microbial ecosystem model which shows alternate stable states. Diamond shaped boxes represent microbial functional groups and circles represent substrates. CB: Cyanobacteria, PB: Phototrophic sulfur bacteria, SB: Sulfate reducing bacteria, P: Phosphorus, O: Oxygen, S_R: Reduced sulfur and S_O: Oxidized sulfur. Dark blue arrows denote consumption of a chemical by the microbial population that they point to. Red arrows denote production of a chemical by the microbial population that they originate from. Orange lines from a chemical to a microbial population represent growth inhibition of the microbial population by that substrate. The green arrow denotes the abiotic reaction of reduced sulfur and oxygen to produce oxidized sulfur.

Figure 5

Evidence for alternate stable states in our mathematical model represented by sensitivity to the initial cyanobacterial population density. We use a log scale for the time axis to visualize the fact that different processes in the system occur on different timescales. For all plots initial $n_{PB} = n_{SB} = 1 \times 10^{11}$ and $S_{O,B} = S_{R,B} = 500\mu M$, $P_B = 0.5\mu M$, $O_B = 300.0\mu M$. (a) shows the dynamics of the model for an initial $n_{CB} = 1 \times 10^5$. (b) shows the dynamics of the model for an initial $n_{CB} = 1 \times 10^9$. The plot shows population densities as a function of time: Green $= n_{CB}$, Orange $= n_{PB}$ and Purple $= n_{SB}$. In (a) the model predicts a final state with coexisting sulfate-reducing bacteria dn phototrophic sulfur bacteria; in (b) it predicts a final state with only cyanobacteria.

Figure 6

Hysteresis in a nutrient-cycling microbial community. (a) Predictions of our mathematical model. The results show the effect of increasing and then decreasing the oxygen diffusivity (see orange arrows) where the initial state of each simulation is set to the final microbial ecosystem state of the previous simulation. The forward and reverse trajectories do not follow the same path. (b) Evidence for regime shifts between oxic and anoxic states in lake Vechten. Hysteresis in the strength of lake stratification as a function of oxygen saturation at 7m depth, from March 2013 (blue square) to April 2014 (red square), following the red arrows. Again the forward and reverse trajectories follow different paths; the system becomes temporarily stuck in a mixed anoxic state.
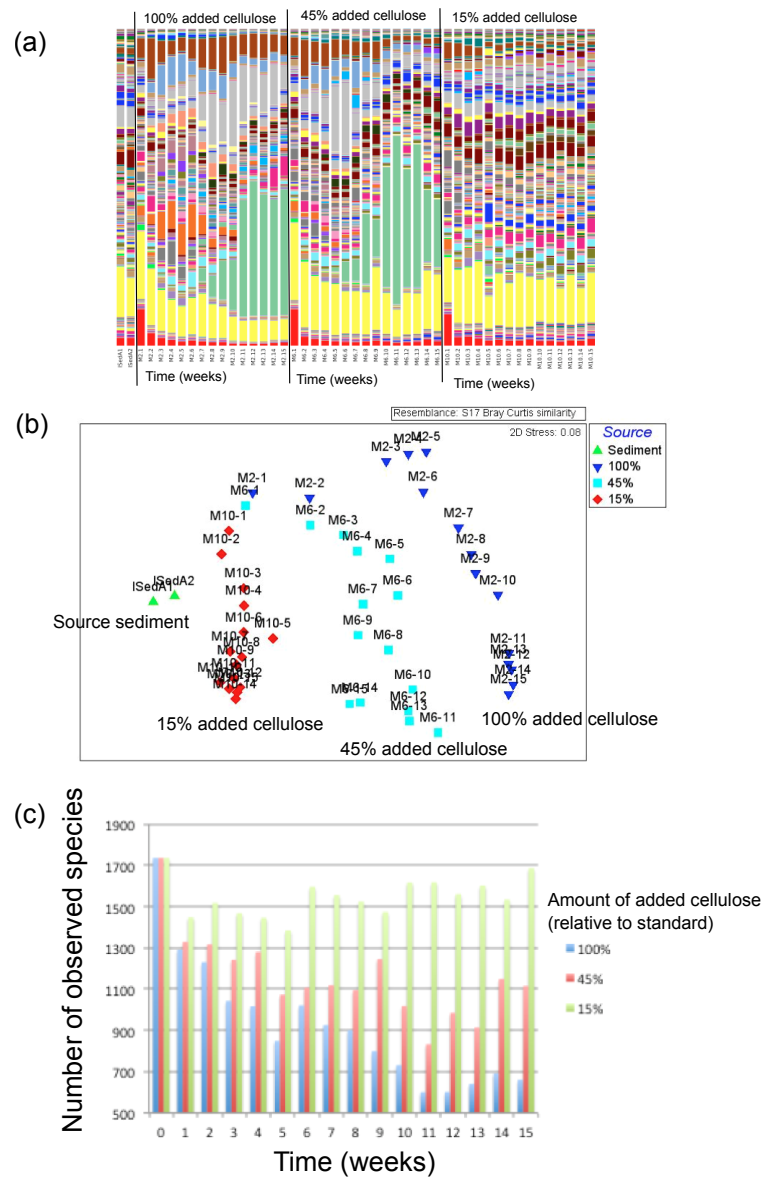
Figure 7

Community composition of our microcosms as a function of time, during the process of community assembly, as assessed by 16S rRNA gene sequencing. Microcosms have been sampled weekly, for 3 different initial concentrations of added cellulose, here denoted 100%, 45% and 15% (relative to a standard). (a): Community composition at the phylum level. Different colors represent different phyla. The left 2 bars show the initial pond sediment used to create the microcosms. (b) The same data, represented on an NMDS plot, where the distance between two points approximates the difference in composition between two samples. It can clearly be seen that microcosms with different initial amounts of cellulose follow different trajectories of community composition. (c) Community species diversity, as measured by the number of observed taxa, as a function of time, for three microcosms with differing amounts of added cellulose.

Phototrophic sulfur bacteria

Sulfate reducing bacteria

Oxygenic phototrophic bacteria
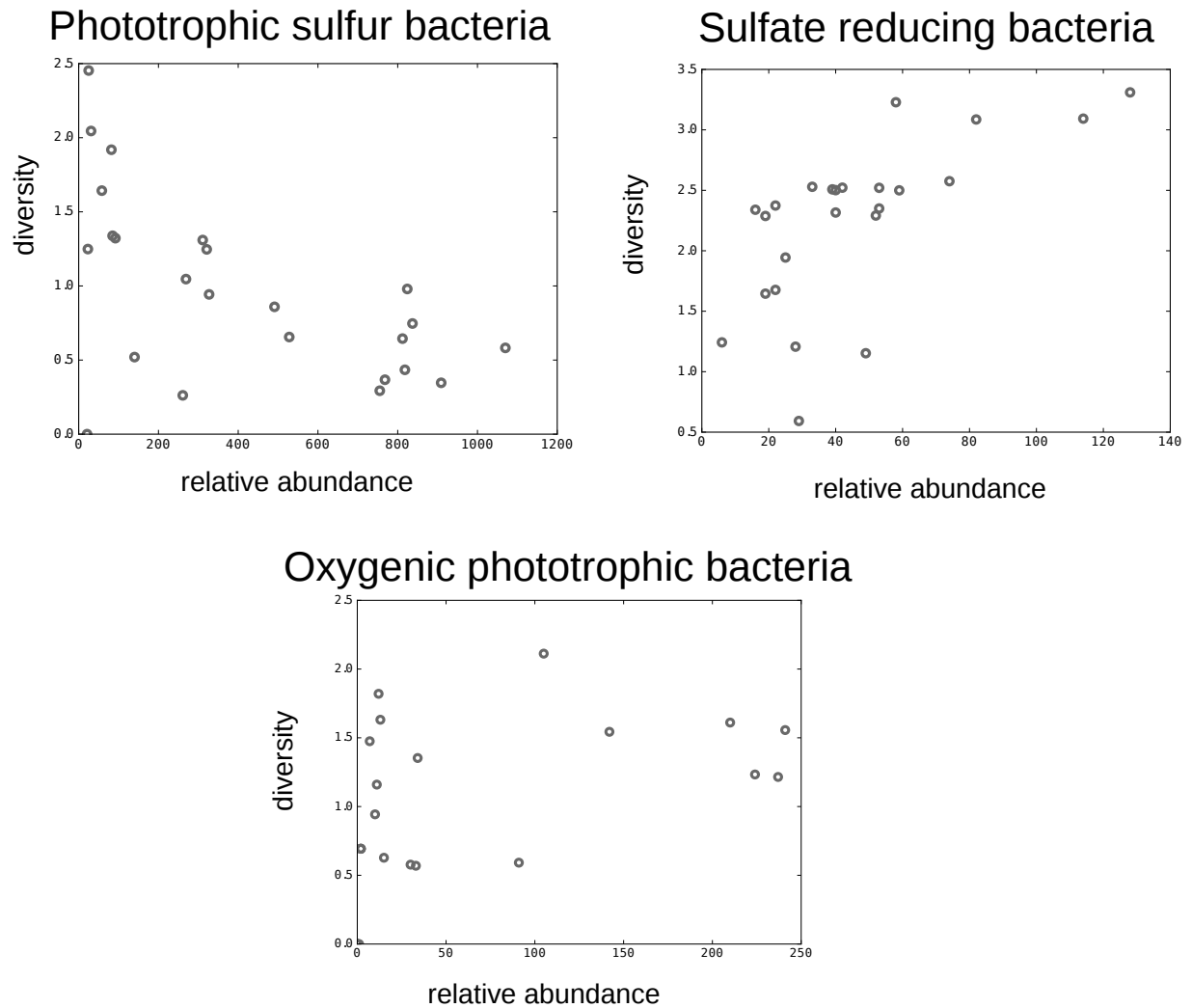
Figure 8

Results from our microcosm experiments with different amounts of added cellulose and sulfate. For three functional groups of bacteria (as defined by taxonomic classification), we plot the diversity (as measured by Shannon Index) as a function of the relative abundance of individual taxa (determined at the 97% level). The three microbial functional groups show very different trends in diversity-abundance relation.
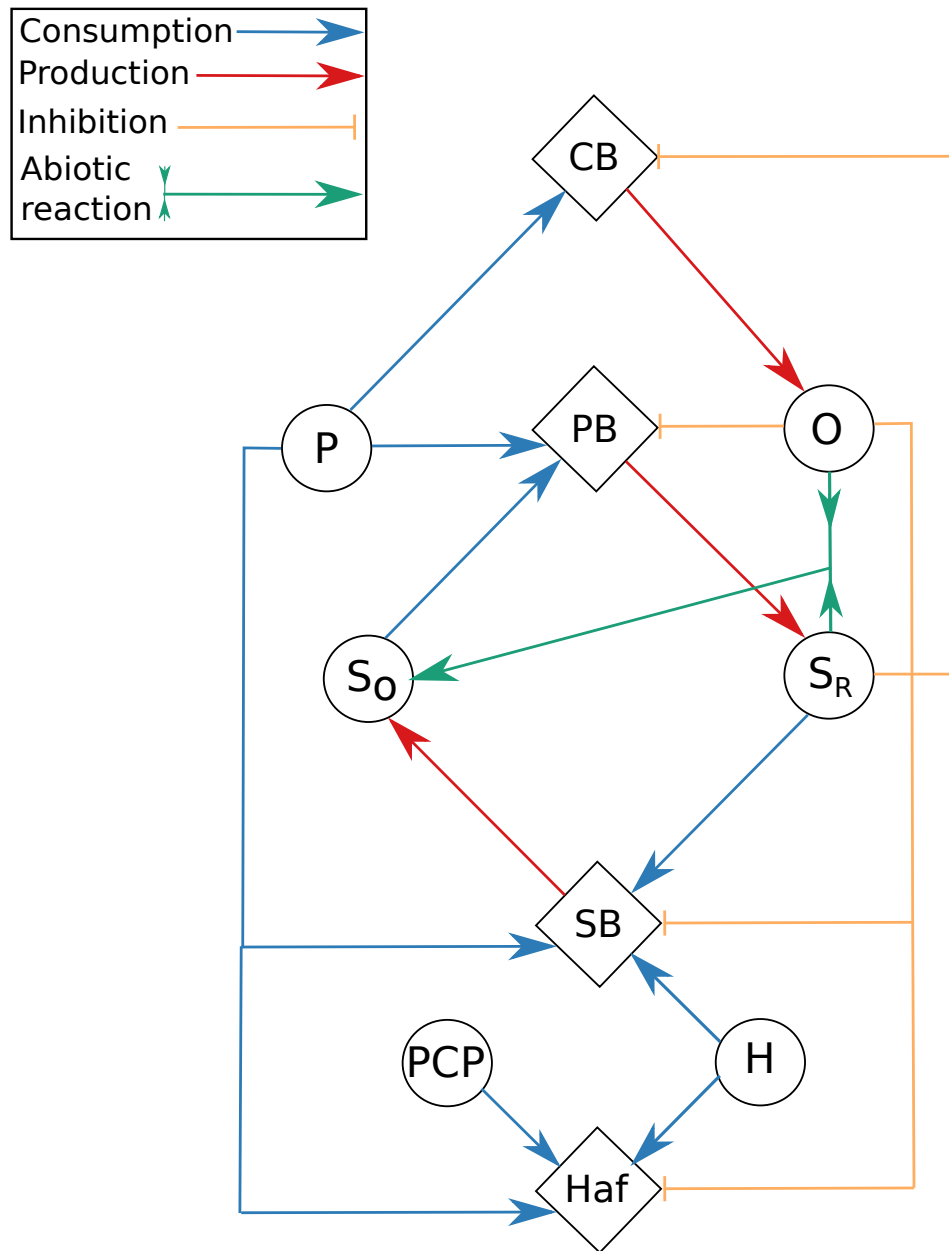
Figure 9

Schematic illustration of our mathematical model for a microbial nutrient-cycling ecosystem supplemented by reductive dehalogenators. Symbols are as in Figure 4. Haf represents the population of *D. Hafniense*, H represents hydrogen and PCP represents the pollutant PCP.
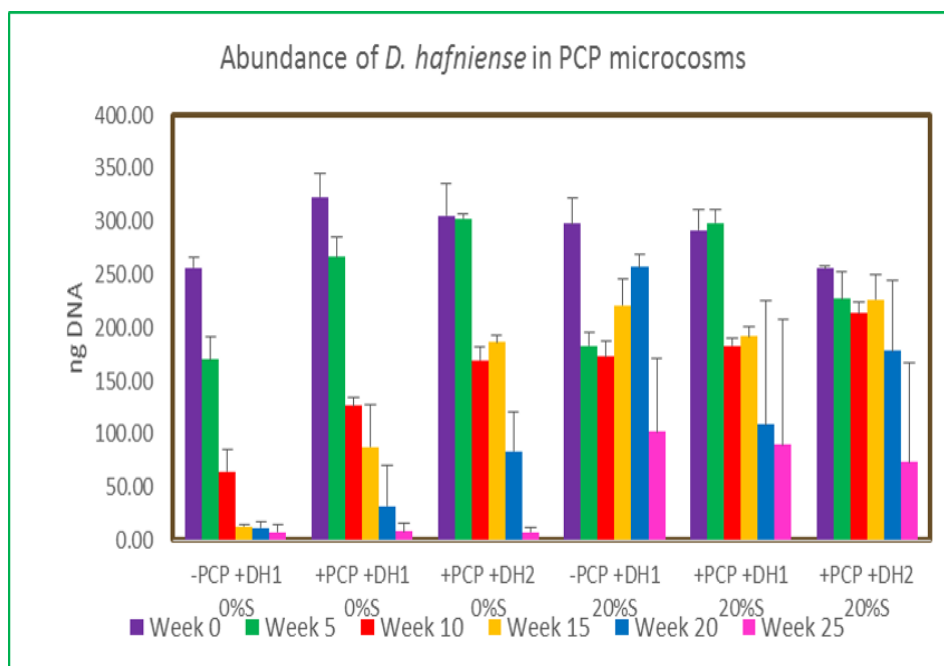
Figure 10

Results of our bioremediation experiment. In this experiment, microcosms were set up with and without addition of the chemical pollutant PCP, with and without addition of sulfate. Microcosms were also supplemented with the PCP-degrading organism *D. hafniense PCP-1*, either at the start only (DH1 in the plot) or both at the start and after 1 month (DH2 in the plot). The abundance of *D. hafniense PCP-1* was monitored by RTPCR at different times, with the results shown by the colored bars. Our results show that in microcosms that are not supplemented by sulfate (left 3 datasets), *D. hafniense PCP-1* dies out over time. However, in microcosms that are supplemented by sulfate (right 2 datasets), *D. hafniense PCP-1* is maintained in the community over much longer times. This suggests that understanding nutrient cycling can provide strategies for successful bioremediation via bioaugmentation.

Appendix 1: The four-population, two-box model

Here we list the equations corresponding to the four-population, two-box model illustrated in Fig. 3.

$$\frac{dn_P(t)}{dt} = \frac{v_P n_P(t) L}{K_L + L}\left(1 - \frac{n_P(t)}{n_{P,\max}}\right) - dn_P(t) \tag{1}$$

Eq. (1) describes growth of the photosynthesizer population, with density n_P. Photosynthesizers are located in the upper box. They grow in response to light intensity L (which is a constant parameter in our model), with maximal growth rate v_P and half-saturation constant K_L. We impose a population size limitation term with maximal population size $n_{P,\max}$ and a death rate d.

$$\frac{dn_D(t)}{dt} = \frac{v_D n_D(t) C}{K_C + C}\left(1 - \frac{n_D(t)}{n_{D,\max}}\right) - dn_D(t) \tag{2}$$

Eq. (2) describes growth of the decomposer population, with density n_D. Decomposers are located in the lower box. They grow in response to organic carbon concentration C (which is a constant parameter in our model), with maximal growth rate v_D and half-saturation constant K_C. We impose a population size limitation term with maximal population size $n_{D,\max}$ and a death rate d.

$$\frac{dn_{or}(t)}{dt} = v_{or} n_{or}(t)\left[\frac{s_o^d(t)}{K_{or} + s_o^d(t)}\right]\left[\frac{a(t)}{a(t) + K_{ac}}\right]\left(1 - \frac{n_{or}(t)}{n_{or,\max}}\right) - dn_{or}(t) \tag{3}$$

Eq. (3) describes growth of the microbial reducer population, with density n_{or}. Reducers are located in the lower box. Reducer growth requires both the oxidized form of the redox chemical species, s_o, and acetate. We describe this using multiplicative Monod terms, with maximal growth rate v_{or} and half-saturation constants K_{or} for s_o and K_{ac} for acetate. The concentration of acetate is denoted as $a(t)$. The reducer population size is limited to $n_{or,\max}$ and we impose a death rate d.

$$\frac{dn_{ro}(t)}{dt} = v_{ro} n_{ro}(t)\left[\frac{s_r^u(t)}{K_{ro} + s_r^u(t)}\right]\left[\frac{o(t)}{o(t) + K_{ox}}\right]\left(1 - \frac{n_{ro}(t)}{n_{ro,\max}}\right) - dn_{ro}(t) \tag{4}$$

Eq. (4) describes growth of the microbial oxidizer population, with density n_{ro}. Oxidizers are located in the upper box. Oxidizer growth requires both the reduced form of the redox chemical species, s_r, and oxygen. Again, we describe this using multiplicative Monod terms, with maximal growth rate v_{ro} and half-saturation constants K_{ro} for s_r and K_{ox} for oxygen. The concentration of oxygen is denoted as $o(t)$. The oxidizer population size is limited to $n_{ro,\max}$ and we impose a death rate d.

$$\frac{do(t)}{dt} = \gamma_{ox} v_P n_P(t)\left[\frac{L}{K_L + L}\right]\left(1 - \frac{n_P(t)}{n_{P,\max}}\right) - \gamma v_{ro} n_{ro}(t)\left[\frac{s_r^u(t)}{K_{ro} + s_r^u(t)}\right]\left[\frac{o(t)}{o(t) + K_{ox}}\right]\left(1 - \frac{n_{ro}(t)}{n_{ro,\max}}\right) - \beta_{ox} o(t) \tag{5}$$

Eq. (5) describes the dynamics of the oxygen concentration. Oxygen is assumed to be located only in the upper box. Oxygen is produced upon growth of the photosynthesizers (first term in Eq. (5)), with yield parameter γ_{ox} (number of micromoles of oxygen produced per bacterial division cycle). Oxygen is consumed upon growth of the oxidizer population (second term in Eq. (5)), with yield parameter γ. We also include a term describing consumption of oxygen by other processes, not included in the model (third term in Eq. (5)), such as growth of aerobes or abiotic oxidation reactions. The parameter β_{ox} controls the strength of this "competition" term.

$$\frac{da(t)}{dt} = \gamma_{ac} v_D n_D(t)\left[\frac{C}{K_C + C}\right]\left(1 - \frac{n_D(t)}{n_{D,\max}}\right) - \gamma v_{or} n_{or}(t)\left[\frac{s_o^d(t)}{K_{or} + s_o^d(t)}\right]\left[\frac{a(t)}{a(t) + K_{ac}}\right]\left(1 - \frac{n_{or}(t)}{n_{or,\max}}\right) - \beta_{ac} a(t) \tag{6}$$

Eq. (6) describes the dynamics of the acetate concentration. Acetate is assumed to be located only in the lower box. Acetate is produced upon growth of the decomposers (first term in Eq. (6)), with yield parameter γ_{ac}. Acetate is

consumed upon growth of the reducer population (second term in Eq. (6)), with yield parameter γ (here assumed to be the same as that of the reducers). We also include a "competition" term describing consumption of acetate by other processes (third term in Eq. (6)), such as growth of methanogens. The parameter β_{ac} controls the strength of this term.

$$\frac{ds_{\mathrm{o}}^{\mathrm{u}}(t)}{dt} = \gamma v_{\mathrm{ro}} n_{\mathrm{ro}}(t) \left[\frac{s_{\mathrm{r}}^{\mathrm{u}}(t)}{K_{\mathrm{ro}} + s_{\mathrm{r}}^{\mathrm{u}}(t)}\right] \left[\frac{o(t)}{o(t) + K_{\mathrm{ox}}}\right] \left(1 - \frac{n_{\mathrm{ro}}(t)}{n_{\mathrm{ro,max}}}\right) + k s_{\mathrm{o}}^{\mathrm{d}}(t) - k s_{\mathrm{o}}^{\mathrm{u}}(t) \tag{7}$$

$$\frac{ds_{\mathrm{o}}^{\mathrm{d}}(t)}{dt} = -\gamma v_{\mathrm{or}} n_{\mathrm{or}}(t) \left[\frac{s_{\mathrm{o}}^{\mathrm{d}}(t)}{K_{\mathrm{or}} + s_{\mathrm{o}}^{\mathrm{d}}(t)}\right] \left[\frac{a(t)}{a(t) + K_{\mathrm{ac}}}\right] \left(1 - \frac{n_{\mathrm{or}}(t)}{n_{\mathrm{or,max}}}\right) + k s_{\mathrm{o}}^{\mathrm{u}}(t) - k s_{\mathrm{o}}^{\mathrm{d}}(t) \tag{8}$$

$$\frac{ds_{\mathrm{r}}^{\mathrm{u}}(t)}{dt} = -\gamma v_{\mathrm{ro}} n_{\mathrm{ro}}(t) \left[\frac{s_{\mathrm{r}}^{\mathrm{u}}(t)}{K_{\mathrm{ro}} + s_{\mathrm{r}}^{\mathrm{u}}(t)}\right] \left[\frac{o(t)}{o(t) + K_{\mathrm{ox}}}\right] \left(1 - \frac{n_{\mathrm{ro}}(t)}{n_{\mathrm{ro,max}}}\right) + k s_{\mathrm{r}}^{\mathrm{d}}(t) - k s_{\mathrm{r}}^{\mathrm{u}}(t) \tag{9}$$

$$\frac{ds_{\mathrm{r}}^{\mathrm{d}}(t)}{dt} = \gamma v_{\mathrm{or}} n_{\mathrm{or}}(t) \left[\frac{s_{\mathrm{r}}^{\mathrm{d}}(t)}{K_{\mathrm{or}} + s_{\mathrm{r}}^{\mathrm{d}}(t)}\right] \left[\frac{a(t)}{a(t) + K_{\mathrm{ac}}}\right] \left(1 - \frac{n_{\mathrm{or}}(t)}{n_{\mathrm{or,max}}}\right) + k s_{\mathrm{r}}^{\mathrm{u}}(t) - k s_{\mathrm{r}}^{\mathrm{d}}(t) \tag{10}$$

Eqs. (7)-(10) describe the dynamics of the reduced and oxidized forms of the redox chemical species, s_{r} and s_{o}, in the upper and lower boxes.

These equations were solved numerically for the steady state, using Euler integration, to obtain the data shown in Fig. 3.

Appendix 2: Description of the mathematical model for a nutrient-cycling ecosystem showing alternate stable states

We model a microbial ecosystem containing three microbial functional groups: oxygen-producing cyanobacteria (CB), phototrophic sulfur bacteria (PB) such as purple or green sulfur bacteria that oxidize reduced sulfur and produce oxidized sulfur, and sulfate-reducing bacteria (SB) that reduce oxidized sulfur and produce reduced sulfur. The dynamics of our mathematical model are controlled by feedbacks between the three functional groups. The oxygen produced by the cyanobacteria is assumed to be inhibitory to both the sulfate-reducing bacteria and phototrophic sulfur bacteria. Conversely, the reduced sulfur produced by the sulfate-reducing bacteria is assumed to be toxic to cyanobacteria. Reduced sulfur is oxidized by the phototrophic sulfur bacteria, and oxidized sulfur is reduced by the sulfate-reducing bacteria, connecting these species in a nutrient cycle as they pass the sulfur back and forth. Importantly, the oxidation of reduced sulfur can also occur abiotically, producing oxidized sulfur in the process.

The dynamics of this model are described by Eqs. 1-7. Eqs. 1-3 describe the dynamics of the cyanobacteria, phototrophic sulfur bacteria and sulfate-reducing bacteria respectively, with population densities represented by n_{CB}, n_{PB} and n_{SB} respectively. For all functional groups a constant removal rate D is applied (e.g. due to grazing or viral lysis). G_i and I_i represent growth and inhibition functions respectively for population i. The growth of each population is assumed to depend on the availability of phosphorus, a key limiting resource of microbial ecosystems in many aquatic environments. Additionally, the growth of the phototrophic sulfur bacteria depends on the availability of reduced sulfur and the growth of sulfate-reducing bacteria depends on the availability of oxidized sulfur.

$$\frac{\mathrm{d}n_{\mathrm{CB}}}{\mathrm{d}t} = n_{\mathrm{CB}}G_{\mathrm{CB}}(P)I_{\mathrm{CB}}(S_{\mathrm{R}}) - Dn_{\mathrm{CB}} \tag{1}$$

$$\frac{\mathrm{d}n_{\mathrm{PB}}}{\mathrm{d}t} = n_{\mathrm{PB}}G_{\mathrm{PB}}(P, S_{\mathrm{R}})I_{\mathrm{PB}}(O) - Dn_{\mathrm{PB}} \tag{2}$$

$$\frac{\mathrm{d}n_{\mathrm{SB}}}{\mathrm{d}t} = n_{\mathrm{SB}}G_{\mathrm{SB}}(P, S_{\mathrm{O}})I_{\mathrm{SB}}(O) - Dn_{\mathrm{SB}} \tag{3}$$

Eqs. 4-7 describe the dynamics of the substrates: oxidized sulfur, reduced sulfur, oxygen and phosphorus respectively. S_{O} represents the concentration of oxidized sulfur and S_{R} represents the concentration of reduced sulfur. O represents the concentration of oxygen and P represents the concentration of freely available phosphorus. For every chemical substrate a background concentration is imposed (labelled by subscript b). The substrate concentration tends to be restored to this background concentration at a rate that depends on the difference between the current concentration and the background concentration, and on a parameter α. The parameter α is specific to each substrate, for example α_{O} controls the rate at which oxygen enters or leaves the system (which in the environment could represent seasonal temperature-related changes in oxygen diffusivity). Importantly, we also include the chemical oxidation of reduced sulfur, which proceeds at a rate $R = -k_2 S_{\mathrm{R}}O$, consuming oxygen (O) and producing oxidized sulfur (S_{O}) in the process.

$$\frac{\mathrm{d}S_{\mathrm{O}}}{\mathrm{d}t} = Y_{\mathrm{PB}}^{S_{\mathrm{O}}}n_{\mathrm{PB}}G_{\mathrm{PB}}(P, S_{\mathrm{R}})I_{\mathrm{PB}}(O) - Y_{\mathrm{SB}}^{S_{\mathrm{O}}}n_{\mathrm{SB}}G_{\mathrm{SB}}(P, S_{\mathrm{O}})I_{\mathrm{SB}}(O) + \alpha_{\mathrm{S}}(S_{\mathrm{O,b}} - S_{\mathrm{O}}) + k_2 S_{\mathrm{R}}O \tag{4}$$

$$\frac{\mathrm{d}S_{\mathrm{R}}}{\mathrm{d}t} = -Y_{\mathrm{PB}}^{S_{\mathrm{R}}}n_{\mathrm{PB}}G_{\mathrm{PB}}(P, S_{\mathrm{R}})I_{\mathrm{PB}}(O) + Y_{\mathrm{SB}}^{S_{\mathrm{R}}}n_{\mathrm{SB}}G_{\mathrm{SB}}(P, S_{\mathrm{O}})I_{\mathrm{SB}}(O) + \alpha_{\mathrm{S}}(S_{\mathrm{R,b}} - S_{\mathrm{R}}) - k_2 S_{\mathrm{R}}O \tag{5}$$

$$\frac{\mathrm{d}O}{\mathrm{d}t} = Y_{\mathrm{CB}}^{O}n_{\mathrm{CB}}G_{\mathrm{CB}}(P)I_{\mathrm{CB}}(S_{\mathrm{R}}) + \alpha_{\mathrm{O}}(O_{\mathrm{b}} - O) - k_2 S_{\mathrm{R}}O \tag{6}$$

$$\frac{\mathrm{d}P}{\mathrm{d}t} = -Y_{\mathrm{CB}}^{P}n_{\mathrm{CB}}G_{\mathrm{CB}}(P)I_{\mathrm{CB}}(S_{\mathrm{R}}) - Y_{\mathrm{PB}}^{P}n_{\mathrm{PB}}G_{\mathrm{PB}}(P, S_{\mathrm{R}})I_{\mathrm{PB}}(O)$$
$$- Y_{\mathrm{SB}}^{P}n_{\mathrm{SB}}G_{\mathrm{SB}}(P, S_{\mathrm{O}})I_{\mathrm{SB}}(O) + \alpha_{\mathrm{P}}(P_{\mathrm{b}} - P) \tag{7}$$

One could in principle choose many different forms for the growth and inhibition functions G_i and I_i. We expect our qualitative results to be largely insensitive to the detailed choice of growth and inhibition function. In this work, we have chosen to use Monod functions. Eqs. 8-10 give the growth functions for the cyanobacteria (G_{CB}), phototrophic sulfur bacteria (G_{PB}) and sulfate reducing bacteria (G_{SB}) respectively.

$$G_{\mathrm{CB}} = v_{\mathrm{CB}} \frac{P}{K_{\mathrm{P,CB}} + P} \tag{8}$$

$$G_{\mathrm{PB}} = v_{\mathrm{PB}} \left(\frac{S_{\mathrm{R}}}{K_{\mathrm{R}} + S_{\mathrm{R}}} \right) \left(\frac{P}{K_{\mathrm{P,PB}} + P} \right) \tag{9}$$

$$G_{\mathrm{SB}} = v_{\mathrm{SB}} \left(\frac{S_{\mathrm{O}}}{K_{\mathrm{O}} + S_{\mathrm{O}}} \right) \left(\frac{P}{K_{\mathrm{P,SB}} + P} \right) \tag{10}$$

In Eqs. 8-10, the microbial growth rate as a function of substrate concentration is described by a Monod function of the form $v \frac{j}{K_j + j}$ where v (hr^{-1}) is the maximal growth rate and K_j (μM) is the concentration of substrate j at which the growth rate is half the maximal growth rate. For functional groups that are limited by the availability of more than one nutrient (the phototrophic sulfur bacteria and the sulfate-reducing bacteria) multiplicative Monod kinetics of the form $v \left(\frac{i}{K_i + i} \right) \left(\frac{j}{K_j + j} \right)$ are used.

Eqs. 11-13 describe the inhibition functions for the cyanobacteria (I_{CB}), phototrophic sulfur bacteria (I_{PB}) and sulfate-reducing bacteria (I_{SB}) respectively. The inhibition of microbial growth is described by a version of the well-known Haldane equation $\frac{1}{1 + \frac{i}{K_i}}$.

$$I_{\mathrm{CB}} = \frac{1}{\left(1 + \frac{S_{\mathrm{R}}}{K_{\mathrm{I,CB}}} \right)} \tag{11}$$

$$I_{\mathrm{PB}} = \frac{1}{\left(1 + \frac{S_{\mathrm{O}}}{K_{\mathrm{I,PB}}} \right)} \tag{12}$$

$$I_{\mathrm{SB}} = \frac{1}{\left(1 + \frac{S_{\mathrm{O}}}{K_{\mathrm{I,SB}}} \right)} \tag{13}$$